Crystallographic Studies of Isosteric NAD Analogues Bound to Alcohol Dehydrogenase: Specificity and Substrate Binding in Two Ternary Complexes[†,‡]

Hong Li,[§] Wendy H. Hallows,[§] John S. Punzi,[§] Krzysztof W. Pankiewicz,[∥] Kyoichi A. Watanabe,[∥] and Barry M. Goldstein*[,§]

Department of Biophysics, University of Rochester Medical Center, Rochester, New York 14642, and Memorial Sloan-Kettering Cancer Center, New York, New York 10021

Received February 24, 1994; Revised Manuscript Received May 26, 1994[⊕]

ABSTRACT: CNAD (5-β-D-ribofuranosylnicotinamide adenine dinucleotide) is an isosteric C-glycosidic analogue of NAD(H) containing a neutral pyridine ring. CPAD (5-β-D-ribofuranosylpicolinamide adenine dinucleotide) is a closely related pyridine-containing analogue with the pyridine nitrogen on the opposite side of the ring. CNAD is a potent and specific inhibitor of horse liver alcohol dehydrogenase (LADH), binding with a dissociation constant in the nanomolar range. CPAD binds LADH with an affinity comparable to that of NAD. Crystal structures of CNAD and CPAD bound to LADH are presented at 2.4 and 2.7 Å, respectively. The two complexes are isomorphous, crystallizing in the triclinic system with cell dimensions different from those seen in previous ternary LADH complexes. Structures were solved using the molecular replacement method and refined to crystallographic *R* values of 18% (CNAD) and 17% (CPAD). Both inhibitors bind to the "closed" form of LADH in the normal cofactor-binding cleft. The conformation of LADH-bound CPAD closely mimics that of LADH-bound NAD(H). The data suggest that alcohol substrate binds directly to the catalytic zinc atom. In the CNAD complex, the pyridine nitrogen replaces alcohol as the fourth coordination ligand to the active site zinc atom, while all other polar interactions remain the same as those of bound NAD(H). The zinc–nitrogen ligand explains the high affinity of CNAD for LADH.

The oxidation of alcohol to aldehyde is one of the rate-limiting steps in ethanol metabolism. This reaction is catalyzed by alcohol dehydrogenase (Crow & Hardman, 1989). Inhibition of this enzyme provides potential therapies for ethylene glycol intoxication (Baud et al., 1987), ethanol-induced hypoglycemia and lactacidemia (Salaspuro et al., 1977), and methanol poisoning (Jacobsen et al., 1990). This, along with available mechanistic and structural information, has made alcohol dehydrogenase an attractive target for rational inhibitor design.

Horse liver alcohol dehydrogenase (LADH,[1] EC 1.1.1.1) is an 80-kDa dimeric NAD-dependent enzyme. The three-dimensional structure of LADH has been well characterized by X-ray crystallography. Structures include that of the apoenzyme, as well as those of a variety of ternary complexes containing both substrate and cofactor analogues (Eklund et al., 1976, 1981, 1984). Recently, the three-dimensional structure of the $\beta_1\beta_1$ human alcohol dehydrogenase isoenzyme complexed with NAD has also been obtained (Hurley et al., 1991). The overall structures of the human and horse enzymes are similar, as are the conformations of the bound coenzyme (Hurley et al., 1991).

Alcohol dehydrogenase is a zinc-containing enzyme. Each 40-kDa monomer contains two tetracoordinate zinc cations and one cofactor and one substrate binding site. The "structural" zinc cation is remote from the active site and may play a role in stabilizing protein folding (Eklund & Brändén, 1987a). The "catalytic" zinc is located at the active site, at the junction between the nicotinamide end of the long cofactor binding cleft and the hydrophobic substrate binding pocket (Eklund et al., 1984).

The active site zinc performs several functions associated with the catalytic reaction. Three of the four coordination ligands to the catalytic zinc are from the protein. In the apo form of the enzyme, the fourth coordination site is occupied by water (Eklund et al., 1976). Following the binding of cofactor, the water ligand is displaced by substrate. This is facilitated by a cofactor-induced shift in equilibrium from an "open" to a "closed" conformation of the enzyme (Eklund & Brändén, 1987a). The zinc-bound substrate is anchored close to the cofactor, allowing direct hydride transfer to the C4 atom of the nicotinamide ring. The positively charged cation also stabilizes an alcoholate ion intermediate, facilitating both hydride transfer and the relay of the substrate proton to solvent (Eklund & Brändén, 1987a,b; Kvassman & Pettersson, 1978; Cook & Cleland, 1981; Klinman, 1981; Kvassman et al., 1981; Eklund et al., 1982a; Ehrig et al., 1991).

There are two general classes of ADH inhibitors. One class includes analogues of alcohols and aldehydes. These compounds bind in the substrate pocket, forming a direct ligand to the catalytic zinc. Examples include pyrazole, dimethyl sulfoxide, and a variety of related compounds (Eklund et al., 1981, 1982b; Cedergren-Zeppezauer, 1983; Dahlbom et al., 1974; Tolf et al., 1979; Fries et al., 1979; Sigman et al., 1982; Freudenreich et al., 1984; Miwa et al., 1987).

The second type of ADH inhibitor consists of analogues of the coenzyme NAD (Danenberg et al., 1978; Cedergren-Zappezauer et al., 1982; Woenckhaus & Jeck, 1987; Li et al., 1994) as well as less structurally related compounds (Einarsson, 1974; Biellmann et al., 1979). These inhibitors bind in the

[†] Supported by National Institutes of Health Grants CA 45145 (B.M.G.) and GM 42010 (K.W.P.).

[‡] Crystallographic coordinates have been deposited in the Brookhaven Protein Data Bank under file names 1ADB and 1ADC for the CNAD and CPAD complexes, respectively.

* To whom correspondence should be addressed.

[§] University of Rochester Medical Center.

[∥] Memorial Sloan-Kettering Cancer Center.

[⊕] Abstract published in *Advance ACS Abstracts,* July 15, 1994.

[1] Abbreviations: CNAD, 5-β-D-ribofuranosylnicotinamide adenine dinucleotide; CPAD, 5-β-D-ribofuranosylpicolinamide adenine dinucleotide; NAD, nicotinamide adenine dinucleotide; LADH, horse liver alcohol dehydrogenase; DMSO, dimethyl sulfoxide; SA, simulated annealing.

0006-2960/94/0433-11734$04.50/0

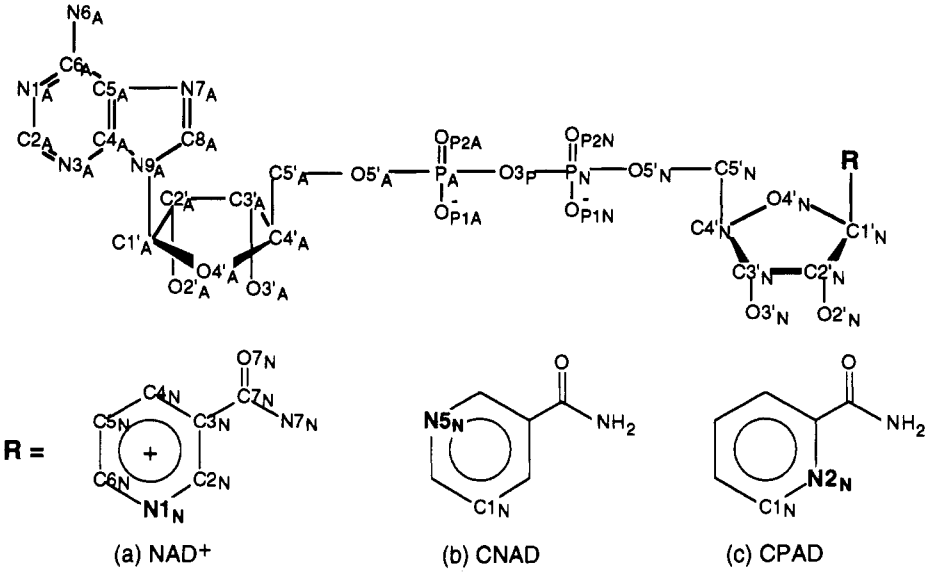

FIGURE 1: Structural formulas and atom labels for (a) NAD^+, (b) CNAD, and (c) CPAD. Atom labels for NAD^+ follow those of Eklund et al. (1984). For comparison, the numbering of the nicotinamide ring is retained in the pyridine rings, and the subscript N is retained for atom labels at the pyridine ends of CNAD and CPAD. Each R group is attached to the ribose $C1'_N$ atom at the 1_N position.

coenzyme binding cleft, generally mimicking binding of the adenosine portion of the cofactor.

5-β-D-Ribofuranosylnicotinamide adenine dinucleotide (CNAD, Figure 1b) is a neutral isosteric analogue of NAD (Pankiewicz et al., 1993). CNAD acts a general dehydrogenase inhibitor, competing with cofactor but resisting hydride reduction (Goldstein et al., 1994). Inhibition constants of CNAD with respect to NAD in malate, lactate, glutamate, and inosine monophosphate dehydrogenases range between 15 and 410 μM (Goldstein et al., 1994; H. N. Jayaram, unpublished results). In these enzymes, binding of CNAD is comparable to that of both normal cofactor and that of other coenzyme analogues (Einarsson, 1974; Abdallah et al., 1975; Biellmann et al., 1979; Goldstein et al., 1990).

In contrast, CNAD shows unusual affinity for LADH. The inhibition constant of CNAD for LADH with respect to NAD is $\sim 4 \times 10^{-3}$ μM (pH 8; Goldstein et al., 1994). This is significantly smaller than the K_i for NADH binding to LADH (0.4 μM) and the K_d for NAD ($\sim$50 μM) (Dalziel & Dickinson, 1975; Goldstein et al., 1994). Further, CNAD competes with both cofactor and substrate binding in LADH ($K_i \sim 2 \times 10^{-3}$ μM) (Goldstein et al., 1994). The affinity of CNAD for LADH is comparable to that of the most potent LADH inhibitors reported (Dahlbom et al., 1974; Tolf et al., 1979; Sigman et al., 1982; Freudenreich et al., 1984; Miwa et al., 1987).

5-β-D-Ribofuranosylpicolinamide adenine dinucleotide (CPAD) is a second isosteric NAD analogue closely related to CNAD (Figure 1c) (Pankiewicz et al., 1993). CPAD also shows competitive inhibition of LADH with respect to NAD but lacks CNAD's high affinity and specificity for the enzyme (Goldstein et al., 1994). CPAD does not compete with substrate binding to LADH and binds to other dehydrogenases with an affinity comparable to that of NAD (Goldstein et al., 1994).

Comparison of kinetic data for CNAD and CPAD indicates that the location of the pyridine nitrogen is crucial in determining inhibitor specificity. Among the enzymes examined, LADH is the only dehydrogenase that contains a zinc cation at the catalytic site. Models of the LADH-bound inhibitors suggest that the pyridine nitrogen of CNAD, but not that of CPAD, sits within potential coordination distance to the catalytic zinc (Goldstein et al., 1994). Thus, it has been hypothesized that the observed specificity of CNAD for LADH is due to a specific interaction between the catalytic zinc atom on the enzyme and the pyridine nitrogen of CNAD (Goldstein et al., 1994).

In order to test this hypothesis, crystal structures of ternary complexes between LADH, alcohol, and both CNAD and CPAD have been determined at 2.4 and 2.7 Å, respectively. Results indicate that binding of CPAD to LADH is identical to that of NAD. In contrast, CNAD acts as a "hybrid" LADH inhibitor, displacing both cofactor and substrate.

EXPERIMENTAL PROCEDURES

(*a*) *Crystals and Data Collection.* CNAD and CPAD were prepared as described by Pankiewicz et al. (1993). Horse liver ADH was obtained as a crystalline suspension from Boehringer Mannheim (Indianapolis, IN). Purity was verified by electrophoresis. Protein solutions were prepared by a modification of methods described previously (Zeppezauer et al., 1967). Briefly, 10 mg of the crystalline suspension was pelleted by centrifugation, and the supernatant was discarded. The pellet was suspended in 500 μL of 50 mM Tris buffer at pH 9.4 $\pm$ 0.1 (+5 °C) and dialyzed against 20 mL of the same buffer for at least 24 h. The dissolved protein was brought to 50 mM Tris at pH 8.4 $\pm$ 0.1 (+5 °C) and 4% (v/v) ethanol by dialysis. The protein concentration was adjusted to $\sim$20 mg/mL by ultrafiltration in a Microcon 10 (Amicon, Beverly, MA). A 10-fold molar excess of inhibitor was added to the concentrated protein, and the solution was filtered through a 0.45-μm cellulose acetate filter (Costar, Cambridge, MA). LADH crystals were obtained by vapor diffusion of 4-μL hanging drops against 10–17% (v/v) ethanol in 50 mM Tris at pH 8.4 $\pm$ 0.1 (+5 °C). Crystals typically appeared in 2–3 days and reached maximal size in 7 days. Typical crystal sizes were 0.1 mm $\times$ 0.2 mm $\times$ 0.4 mm. Crystals were sealed in glass capillary tubes with mother liquor for data collection.

X-ray diffraction data were collected from a single crystal of the LADH–CNAD complex on a Xentronics area detector with a Cu rotating anode X-ray source operating at 50 mA and 60 kV. The crystal temperature was maintained at 4 $\pm$ 1 °C throughout the data collection. The detector was set at $2\theta = 22°$ with a crystal-to-detector distance of 12 cm. Data were obtained from a single setting using an oscillation angle

Table 1: Summary of Crystal and Diffraction Data

	LADH–CPAD	LADH–CNAD[b]
crystal system	triclinic	triclinic
space group	*P*1	*P*1
a (Å)[a]	51.9	51.8
b (Å)	44.8	44.6
c (Å)	93.0	93.0
α (deg)	103.1	103.5
β (deg)	87.8	88.1
γ (deg)	70.4	70.4
resolution (d_{min}, Å)	2.7	2.4
$\langle I/\sigma(I)\rangle$ to d_{min}	1.7	2.0
no. of reflections collected	36058	46920
no. of unique reflections	19251	24289
data completeness (%)	92	82
R_{merge} (%)[c]	12.7	9.8

[a] Standard deviations are estimated at 0.2 Å in the axial lengths and 0.3° in interaxial angles on the basis of variations in these parameters refined from succesive blocks of data. [b] Ethanol complex. See text for data from the (*S*)-(+)-2-pentanol complex. [c] $R_{merge} = \sum_{hkl}\sum_i|I^i_{hkl} - \langle I_{hkl}\rangle|/\sum_{hkl}\sum_i I^i_{hkl}$.

of 0.25° in omega and an exposure of 120 s per frame. The LADH–CNAD crystals provided useful data to 2.4 Å ($\langle I/\sigma(I)\rangle$ = 2.0). Data were processed using XDS software (Kabsch, 1988a,b).

X-ray diffraction data from a single LADH–CPAD crystal were collected under conditions similar to those described above and provided useful data to 2.7 Å ($\langle I/\sigma(I)\rangle$ = 1.7). Diffraction data were also processed using XDS software (Kabsch, 1988a,b). Crystal data and intensity statistics for both complexes are summarized in Table 1.

In order to investigate substrate binding to the LADH–CPAD complex, a ternary complex to LADH–CPAD with a second alcohol having a longer alkyl chain was also examined. (*S*)-(+)-2-pentanol was chosen for this purpose. Crystals of LADH–CPAD–pentanol were obtained by soaking LADH–CPAD–ethanol crystals, grown as described above, in 20% v/v (*S*)-(+)-2-pentanol for a period of 7 days. Diffraction data for the LADH–CPAD–(*S*)-(+)-2-pentanol crystals were then obtained under conditions similar to those for the isomorphous LADH–CPAD–ethanol complex. Pentanol-soaked crystals provided 13 391 reflections to 2.9 Å (13 282 unique, $\langle I/\sigma(I)\rangle$ = 2.4; 79% complete, R_{merge} = 9% between the pentanol and ethanol data sets). Diffraction data were processed using XDS software (Kabsch, 1988a,b).

(b) Structure Solution of the LADH–CNAD–Ethanol Complex. The LADH–CNAD–ethanol complex crystallized in the triclinic system (Table 1). There is one dimeric molecule per asymmetric unit. The crystal packing of this complex differs somewhat from that of previously reported triclinic complexes of LADH, resulting in a ~12° decrease in the value of β observed here (Eklund et al., 1982a,b, 1984; Cedergren-Zeppezauer et al., 1982). This difference required the use of the molecular replacement method for structure solution.

The LADH–CNAD–ethanol structure was solved by molecular replacement using LADH from the LADH–NADH–DMSO complex (Eklund et al., 1984) as a search model. Coordinates of the LADH–NADH–DMSO complex were obtained from the Brookhaven Protein Data Bank (Bernstein et al., 1977). Structure solution and refinement were performed using the molecular dynamics program X-PLOR, version 3.0 (Brünger, 1992a). Map display employed the program CHAIN (Sack, 1988).

A self-rotation function search (Huber, 1985) in spherical polar coordinates (ψ, φ, κ) (Rossmann & Blow, 1962) was first performed to locate the noncrystallographic 2-fold axis relating the two monomers of the LADH dimer. A single peak appeared on the search map at ψ = 131.1°, φ = 173.3° and κ = 180° (supplementary material). The orientation of this 2-fold axis is different from that found in earlier triclinic LADH complexes, in which the 2-fold axis lies along the unit cell *b*-axis. The LADH dimer from the LADH–NADH–DMSO complex (Eklund et al., 1984) was then used as a model to perform a cross-rotation search to orient the LADH–CNAD–ethanol dimer in the unit cell. Orientations corresponding to the two strongest peaks from this search (supplementary material) yielded the highest correlation values following a subsequent Patterson correlation (PC) refinement (Brünger, 1990). These two orientations are related by the 2-fold symmetry axis of the LADH–CNAD dimer found in the self-rotation function search.

At this point, the initial model for the enzyme–CNAD complex was obtained by rotating the LADH dimer from the LADH–NADH–DMSO structure to the orientation having the highest correlation value from the PC refinement. Euler angles for this orientation are 342.7°, 174.6°, 31.3°. This model was then subjected to the refinement procedure summarized in Table 2.

Electron densities for the bound CNAD molecules were clearly defined after an initial rigid body refinement (Table 2). Each monomer binds one CNAD molecule. In subsequent simulated annealing refinements, CNAD models for both monomers were included (Table 2). Force parameters for the CNAD molecule were modified from those of NAD. However, point charges for the CNAD pyridine ring were obtained from *ab initio* calculations on model fragments.

The simulated annealing (SA) procedure was performed as follows. The system was initially heated to 2000 K and slowly cooled to 300 K in 25 K steps. At each temperature, a 25-fs molecular dynamics run was performed using the *T* coupling strategy (Brünger et al., 1990). This process was followed by 120 steps of conjugate gradient minimization. Ten steps of overall *B*-factor refinement were then performed followed by 20 steps of individual *B*-factor refinement.

The cross-validation procedure was used to monitor the quality of the refinement (Brünger, 1992b). The data were divided into two sets of reflections. One set contained 10% of the original data, chosen in a random fashion. The second set contained the remaining reflections and was used in the refinement. However, crystallographic residuals (R_{free} and *R*, respectively) were computed for both sets. The value of R_{free} is less biased by potentially incorrect models (Brünger, 1992b). Both residuals are listed in Table 2.

$2F_o - F_c$ maps were used to assess the refined models. Weak densities were found in regions mostly on the protein surface. In order to minimize bias introduced by the initial model, residues in these regions were excluded two at a time using a 5-Å radius omitted region in separate SA procedures (Hodel et al., 1992). Free *R* values were calculated for each SA refinement. If a smaller value of R_{free} was obtained, the omitted residues were remodeled into new $2F_o - F_c$ omit maps.

Water molecules were identified on the basis of the presence of (1) a peak on the $F_o - F_c$ map at the 2.5σ level, (2) a peak at the same location on the $2F_o - F_c$ map at the 1σ level, and (3) a reasonable hydrogen-bonding geometry between the putative solvent molecule and a protein residue, the inhibitor, and/or another water molecule. Fifty-six water molecules were included in the final model.

Following SA, a large peak was initially observed on the $F_o - F_c$ map (2.5σ) in both monomers in the substrate binding

Table 2: Summary of Refinement Procedures and Results for LADH Ternary Complexes

step	R^a	R_{free}	model	RMS values: bond length (Å)	bond angle (deg)	dihedral angle (deg)	improper angle (deg)
			LADH–CNAD–Ethanol Complex				
1. rigid body refinement	0.37	0.36	LADH				
2. simulated annealing	0.20	0.34	LADH + CNAD	0.019	3.9	26.6	2.3
3. conjugate minimization	0.20	0.32	LADH + CNAD + EtOH + solvent	0.012	2.2	25.7	1.9
4. NCS restrained refinement and increased geometry constraints[b]	0.18	0.28	LADH + CNAD + EtOH + solvent	0.010	1.9	25.1	1.6
			LADH–CPAD–Ethanol Complex[c]				
1. simulated annealing	0.20	0.28	LADH + CPAD	0.015	2.2	25.4	1.9
2. conjugate minimization	0.19	0.30	LADH + CPAD + EtOH + solvent	0.013	2.2	25.5	1.9
3. NCS restrained refinement and increased geometry constraints[b]	0.17	0.28	LADH + CPAD + EtOH + solvent	0.011	1.9	25.1	1.7

[a] Unweighted residual: $R = \sum_{hkl}(|F_o(hkl)| - k|F_c(hkl)|)/\sum_{hkl}|F_o(hkl)|$, where k is the scaling factor. R is calculated for all reflections between 8 Å and d_{min}, except for step 1 (see Experimental Procedures). R values listed are those after each procedure. [b] NCS = noncrystallographic symmetry. Increased geometry constraints are obtained by increasing force constants for bond lengths and angles, torsion angles, and improper torsion angles. The last cycle of this procedure is a conjugate minimization without the NCS restraint. [c] Methods and results for the (*S*)-(+)-2-pentanol complex are similar (see text).

Table 3: Torsion Angles (deg) for LADH-Bound CNAD, CPAD, and NADH

torsion angles[a]	CNAD-A	CNAD-B	CPAD-A	CPAD-B	NADH-A[b]	NADH-B[b]
$\chi_A = C4_A - N9_A - C1'_A - C2'_A$	147	140	144	125	147	136
$\gamma_A = C3'_A - C4'_A - C5'_A - O5'_A$	−92	−75	−69	−82	−79	−99
$\beta_A = C4'_A - C5'_A - O5'_A - P_A$	134	156	132	157	147	136
$\alpha_A = C5'_A - O5'_A - P_A - O3_P$	106	84	97	90	106	104
$\zeta_A = O5'_A - P_A - O3_P - P_N$	85	83	68	82	85	83
$\zeta_N = O5'_N - P_N - O3_P - P_A$	−154	−151	−145	−148	−153	−151
$\alpha_N = C5'_N - O5'_N - P_N - O3_P$	60	65	89	59	59	76
$\beta_N = C4'_N - C5'_N - O5'_N - P_N$	−168	−172	−161	−162	−146	−169
$\gamma_N = C3'_N - C4'_N - C5'_N - O5'_N$	60	47	49	78	39	42
$\chi_N = Y - X - C1'_N - C2'_N$	157	151	137	138	142	139
$\chi'_N = O4'_N - C1'_N - X - Y$	−86	−88	−108	−107	−102	−104
$\kappa_N = O7_N - C7_N - C3_N - C4_N$	2	8	28	14	34	31

[a] For CNAD, X = $C1_N$ and Y = $C2_N$; for CPAD, X = $C1_N$ and Y = $N2_N$; for NADH, X = $N1_N$ and Y = $C2_N$ (see Figure 1). [b] Eklund et al., 1984.

channel, 4 Å from the zinc cation. A single water molecule did not completely account for all of the density. Given the presence of 14% v/v of ethanol in the crystallization medium, this peak was modeled as an ethanol molecule. The hydroxyl oxygen of the ethanol was placed within hydrogen-bonding distance of OG of Ser-48. Following refinement of the model (below), the height of the putative substrate peak on the ethanol-omitted $F_o - F_c$ map was 7σ above background.

Refinement cycles at this stage utilized the parhcsdx.pro and tophcsdx.pro parameter and topology files in order to obtain better RMS values for the protein model (Brünger, 1992a) (Table 2). Examination of the Ramachandran plot at this point showed a number of non-glycine residues in disallowed regions. Further, one subunit (subunit B) showed more residues in disallowed regions than the other (subunit A). Thus, subsequent refinements used a noncrystallographic symmetry (NCS) restraint energy term (Brünger, 1992a). Only backbone atoms of the two subunits were restrained to the approximate 2-fold symmetry of the dimer. Bound ligands were not restrained. The weighting factor on the crystallographic term, W_a, was also reduced by 20% from the value initially supplied by the check procedure (Weis et al., 1990). Following the use of these procedures and some manual adjustment, RMS values for molecular geometries and Ramachandran plots were improved, and values of R_{free} were reduced. In the last cycle of this procedure, a conjugate minimization was performed with all NCS restraints removed. Final residuals and RMS values are listed in Table 2.

(*c*) *Structure Solution of the LADH–CPAD–Ethanol and LADH–CPAD–(S)-(+)-2-Pentanol Complexes.* LADH–CPAD–ethanol crystals are isomorphous with LADH–CNAD crystals. The LADH–CPAD–ethanol complex was solved by using the LADH coordinates from the refined LADH–CNAD–ethanol complex to calculate initial phases. CPAD binding was clearly discerned from the $F_o - F_c$ map calculated using these initial phases. A CPAD molecule was fitted to both $F_o - F_c$ and $2F_o - F_c$ maps, and the LADH–CPAD model was then subjected to the same SA procedure as described for the LADH–CNAD structure. Difference maps were examined, and questionable residues were redefined using the omitted-SA procedure described above. The cross-validation procedure was also carried out during the refinement, and residuals are listed for each stage in Table 2. Twenty-eight water molecules were identified as described above.

A peak on the $F_o - F_c$ map was initially observed at the 2.5σ level 2 Å from the active site zinc in both subunits. Extra density was also observed in the same location of the $2F_o - F_c$ map at 1.0σ. Again, extra $F_o - F_c$ density could not be accounted for at the 2.5σ level by a single water molecule. Thus, this peak was also modeled as an ethanol molecule, the hydroxyl oxygen being placed within coordination distance of the zinc cation. Following refinement of the model, the height of the putative substrate peak on the ethanol-omitted $F_o - F_c$ map was 5σ above background. Alcohol coordination to the catalytic zinc at this site was later confirmed by the pentanol–LADH structure (below).

The final model contained two protein monomers, two CPAD ligands, twenty-eight water molecules, and two methanol molecules in the asymmetric unit. This model was subjected to final conjugate gradient minimization refinements

with a 2-fold noncrystallographic symmetry restraint as described above. Final refinement cycles utilized the parhcsdx.pro and tophcsdx.pro parameter and topology files (Brünger, 1992a). Final residues and RMS values are listed in Table 2.

The structure of the LADH–CPAD–(*S*)-(+)-2-pentanol complex was refined using the LADH–CPAD model from the isomorphous LADH–CPAD–ethanol complex to obtain initial phases. Refinement procedures were similar to those described for the LADH–CPAD–ethanol complex. The structure was refined to a final crystallographic R value of 15%, with final RMS values similar to those obtained for the ethanol complexes listed in Table 2. In the refined structure, the height of the pentanol peak on the alcohol-omitted $F_o - F_c$ map was 6.5σ above background. No additional peaks were observed on this map in the region of the catalytic zinc.

RESULTS

(*a*) *Protein Structures.* Refined LADH molecules in both CPAD and CNAD complexes fit electron densities well in all regions, with the exception of a few surface residues. Luzzati plots (Luzzati, 1952) of the final refined models (supplementary material) indicate average positional errors of 0.25 Å in the CNAD complex and 0.35 Å in the CPAD complex. These assume that positional errors are the sole source of differences in F_o and F_c and that these errors are normally distributed (Luzzati, 1952). Ramachandran plots (Ramachandran & Sasisekharan, 1968) (supplementary material) indicate that the majority of ψ/ϕ angles for the non-glycine residues are reasonable. RMS deviations of the refined models from ideal geometries are indicated in Table 2.

The two LADH complexes are isomorphous. Refined LADH structures in the two complexes were compared by alignment of the Cα carbons. The RMS difference between the two backbones is 0.5 Å, and that between all atoms in the two proteins is 1.0 Å. Catalytic zinc positions in the two complexes differ slightly. The Zn atom in the CNAD complex is shifted 0.9 Å toward the nicotinamide ring of the bound CNAD. The cause of this shift in the catalytic zinc position is discussed below.

Both the LADH–CNAD–ethanol and the LADH–CPAD–ethanol complexes crystallize in the same closed conformation seen in other ternary complexes. However, crystal packing in the CNAD and CPAD complexes is different from that seen in previous LADH triclinic complexes (Eklund et al., 1982a,b, 1984; Cedergren-Zeppezauer et al., 1982). The RMS difference in Cα positions between the LADH structure in the CPAD complex and that in the triclinic LADH–NADH–DMSO complex (Eklund et al., 1984) is 0.5 Å. The RMS difference in all atom positions is 1.0 Å. The largest RMS differences between individual residues are observed for Thr-2 and Thr-122 in subunit B and Asn-259 in both subunits. Orientations of these surface residues differ from those observed in the NADH–DMSO structure and required remodeling during the omitted SA procedure described above. RMS differences between both structural and catalytic zinc atoms in the NADH–DMSO and CPAD–ethanol complexes are within the range of experimental error.

(*b*) *Novel Crystal Packing.* It is clear from the comparisons above that the different packing environment observed in the CPAD and CNAD complexes did not change the overall conformation of the enzyme. However, it is worth pointing out the differences in packing between these complexes and that observed in the previous triclinic LADH–NADH–DMSO structure (Eklund et al., 1984).

In the DMSO triclinic complex, polar interactions are observed between residues 17–18 in one monomer (subunit A) and residues 337–338 in the same subunit of a neighboring dimer. The two dimers are related by a unit cell translation along the *b*-axis (Eklund et al., 1984). In the complexes presented here, polar interactions are observed between residues 297–298 in subunit A and residues 337–338 from the same subunit of the neighboring dimer related by the *b*-axis translation.

Close intermolecular contacts are observed in the LADH–NADH–DMSO structure between residues 218, 233–239, and 242–259 in subunit A and residues 218, 226, 233, and 239–259 in subunit B of the neighboring dimer related by translation along the *a*-axis (Eklund et al., 1984). These contacts are not observed in the CNAD and CPAD complexes. Interactions between the second monomer (subunit B) and its neighbor related by translation along the *b*-axis are conserved in both crystal forms.

(*c*) *CNAD Coordinates with the Active Site Zinc.* Given the unusual specificity and affinity of CNAD for LADH, the conformation of enzyme-bound CNAD is of particular interest. The CNAD-omitted $F_o - F_c$ map in the region of the cofactor binding site of subunit A is shown in Figure 2a. The corresponding map from subunit B is very similar. The conformation of LADH-bound CNAD was compared with that of LADH-bound NADH from the ternary DMSO complex (Eklund et al., 1984) by performing an RMS fit between the LADH backbones in the two complexes. The RMS difference between CNAD and NADH in these two complexes is 0.6 Å. The comparison between the cofactor and inhibitor molecules resulting from this fit is shown in Figure 3a. Torsion angles for LADH-bound NADH and CNAD are compared for each subunit in Table 3.

One CNAD molecule occupies the cofactor binding site on each LADH monomer. The general features of adenosine binding in CNAD are similar to those found in NADH in the LADH–NADH–DMSO complex (Eklund et al., 1984) as well as those of other LADH-bound dinucleotides observed previously (Cedergren-Zeppezauer et al., 1982; Eklund et al., 1982a,b, 1984; Li et al., 1994). The adenine portion of CNAD binds in the hydrophobic pocket between Ile-224 and Ile-269. Difference maps clearly define a 2′-endo–3′-exo pucker for the adenine ribose. The adenine ribose hydroxyl oxygens $O2'_A$ and $O3'_A$ form H-bonds with side chains of Asp-223 and Lys-228 (Table 4a).

The pyrophosphate region of CNAD also forms hydrogen bonds with the protein. O_{P1N} is 3.1 Å from the main-chain nitrogen of Arg-47, which is well-defined in the present structure. O_{P2N} forms H-bonds with main-chain nitrogens of Gly-202 and Val-203 (Table 4a). The same bonds are observed between NADH and LADH in the closed form (Eklund et al., 1984).

The pyridine ribose of CNAD shows the same 2′-endo–3′-exo pucker observed in the adenine ribose. The hydroxyl oxygen, $O2'_N$, forms hydrogen bonds with His-51 NE2 and Ser-48 OG. The same hydrogen-bonding network is observed in LADH-bound NADH, as part of the putative proton relay system between alcohol and solvent (see below) (Kvassman & Pettersson, 1978; Cook & Cleland, 1981; Eklund et al., 1982a; Sekhar & Plapp, 1990; Ehrig et al., 1991). As observed previously, the hydroxyl oxygen $O3'_N$ forms hydrogen bonds with Ile-269 O and Val 294 N (Table 4a) (Eklund et al., 1984). Thus, up to this point in the structure, LADH-bound CNAD shows the same conformation and protein interactions as observed in normal LADH-bound coenzyme.

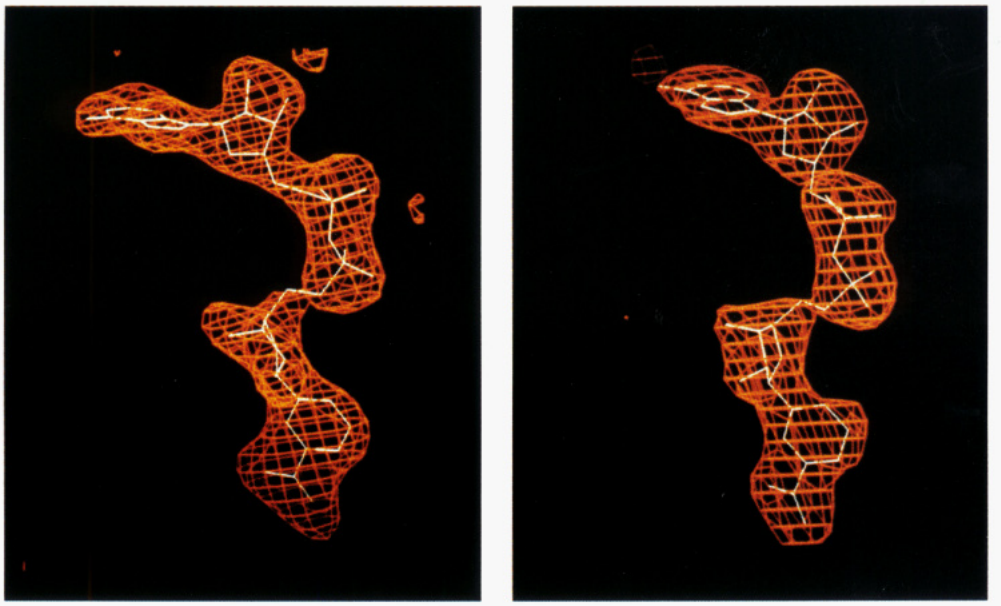

FIGURE 2: $F_o - F_c$ maps of the ligand binding region of subunit A in (a, left) LADH–CNAD and (b, right) LADH–CPAD. Maps were obtained from the final refined LADH models with inhibitors omitted and contoured at the 3.0σ level. CNAD and CPAD models are shown in white. Corresponding maps for each complex from subunit B are very similar.

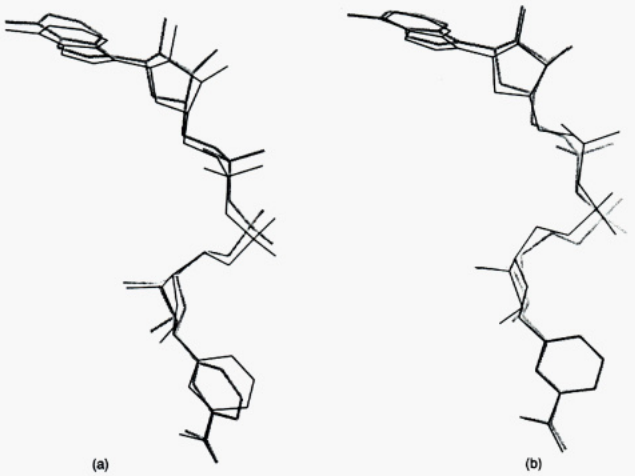

FIGURE 3: Comparison of LADH-bound NADH (thick lines) with (a) LADH-bound CNAD and (b) LADH-bound CPAD (thin lines). The NADH structure is from the LADH–NADH–DMSO complex (Eklund et al., 1984). The overlap was obtained by superposition of the Cα atoms of the LADH–NADH complex with those from the inhibitor complexes.

Differences in conformation between LADH-bound NADH and CNAD are most pronounced at the pyridine rings (Figure 3a). The $2F_o - F_c$ map with CNAD omitted shows continuous density between the pyridine ring and the active site zinc atom (Figure 4a). This feature is not observed in the NADH complex (Eklund et al., 1984) nor in the CPAD complex (Figure 4b, below). Comparison of LADH-bound CNAD and cofactor indicates that the pyridine ring of CNAD is rotated about a virtual axis between $C1_N$ and $C3_N$, such that the pyridine nitrogen $N5_N$ is moved closer to the zinc cation (Figure 5). This results in the observed differences in torsion angles χ_N and κ_N between CNAD and NADH (Table 3). This rotation reduces the $N5_N$–Zn distance to 2.2 Å, considerably shorter than the $C5_N$–Zn distance of 3.6 Å observed in LADH-bound NADH (Eklund et al., 1982a,b, 1984). These results indicate the formation of a coordination ligand between the CNAD pyridine nitrogen and the catalytic zinc cation.

Despite the rotation of the pyridine ring due to the $N5_N$···Zn attraction, the carboxamide group of CNAD forms the same hydrogen bonds as those formed by the nicotinamide group in LADH-bound NADH (Eklund & Brändén, 1984). The carboxamide amino group on CNAD hydrogen bonds to the carbonyl oxygens of residues 292 and 317. The carboxamide oxygen hydrogen bonds to the main-chain nitrogen of residue 319 (Table 4a, Figure 4a). In normal cofactor binding, these hydrogen bonds are crucial for the proper positioning of the nicotinamide end of the molecule. Formation of these bonds may also be required for the transformation from the open to the closed form of the enzyme (Eklund & Brändén, 1987a). Binding of NAD analogues lacking the carboxamide group fails to induce the conformational change to the closed form (Samama et al., 1977, 1981; Eklund et al., 1984; Eklund & Brändén, 1987a). Conservation of the carboxamide hydrogen bonds in the LADH–CNAD complex likely contributes to the maintenance of the closed-form conformation observed in this complex.

Formation of the carboxamide group hydrogen bonds discussed above does limit the movement of the CNAD pyridine ring. The rotation of the pyridine ring observed in CNAD would not by itself be sufficient to bring the $N5_N$ atom within coordination distance of the catalytic zinc. The Zn···N coordination is further facilitated by a shift of the entire Zn coordination sphere toward the $N5_N$ atom. The catalytic zinc atom in the LADH–CNAD complex is shifted by 0.9 Å toward the pyridine ring, relative to its position in the LADH–NADH complex (Figure 5), and by 0.7 Å, relative to its position in the LADH–CPAD complex (below).

In spite of the shift of the catalytic zinc, the coordination geometry in the LADH–CNAD complex is similar to that in both the LADH–NADH and LADH–CPAD complexes (Table 5). This indicates that the motion at the active site zinc in the LADH–CNAD complex is accompanied by motion in the ligands of the coordination sphere (Figure 5).

In other LADH structures, the fourth coordination ligand of the active site Zn is occupied by water, substrate, or substrate analogues (Eklund et al., 1976, 1982a, 1984; Ramaswamy et al., 1994). In the CNAD complex, coordination to the pyridine $N5_N$ atom displaces the solvent–Zn ligand normally seen

Table 4: List of Contacts between CNAD and LADH and between CPAD and LADH within 3.2 Å

(a) Contacts between CNAD and LADH

LADH	CNAD	D (Å)[a]	type of contact
Arg-47 N	O_{P1N}	3.1/3.1	H-bond
Arg-47 CD	O_{P1A}	3.2/2.9	VDW
Arg-47 NH1	O_{P1A}	3.0/2.9	H-bond
Ser-48 OG	$O2'_N$	2.9/3.0	H-bond
Ser-48 OG	$C6_N$	3.3/3.0	VDW
His-51 CD2	$O2'_N$	2.9/2.9	VDW
His-51 NE2	$O2'_N$	2.9/2.8	H-bond
His-51 NE2	$O3'_N$	3.4/2.9	H-bond
Gly-202 N	O_{P2N}	3.5/3.2	H-bond
Val-203 N	O_{P2N}	3.1/3.0	H-bond
Val-203 CG2	O_{P2N}	3.3/3.2	VDW
Asp-223 OD1	$O3'_A$	3.0/2.8	H-bond
Asp-223 OD2	$O2'_A$	2.8/2.6	H-bond
Lys-228 NZ	$O3'_A$	3.2/2.8	H-bond
Val-268 O	$C5'_N$	3.2/3.6	VDW
Ile-269 O	$O3'_N$	2.6/2.7	H-bond
Val-292 O	$C2_N$	3.1/3.4	VDW
Val-292 O	$N7_N$	3.0/3.0	H-bond
Val-294 N	$O3'_N$	3.2/3.1	H-bond
Ala-317 O	$N7_N$	3.1/3.1	H-bond
Phe-319 N	$O7_N$	3.1/3.1	H-bond
Arg-369 NH1	O_{P1N}	3.0/2.9	H-bond
Zn(I)	$C6_N$	3.1/3.2	VDW
Zn(I)	$N5_N$	2.2/2.2	coordination
WAT-22 O[b]	O_{P2N}	—/3.0	H-bond

(b) Contacts between CPAD and LADH

LADH	CPAD	D (Å)[a]	type of contact
Arg-47 N	O_{P1N}	3.3/3.1	H-bond
Arg-47 CB	$O3_P$	3.0/3.1	VDW
Arg-47 NH1	O_{P1A}	2.9/2.6	H-bond
Ser-48 OG	$O2'_N$	3.1/3.9	H-bond
His-51 CD2	$O2'_N$	3.2/2.8	VDW
His-51 NE2	$O2'_N$	3.2/2.8	H-bond
His-51 NE2	$O3'_N$	3.0/2.9	H-bond
Gly-202 N	O_{P2N}	3.4/3.1	H-bond
Val-203 N	O_{P2N}	3.2/3.2	H-bond
Val-203 CG2	O_{P2N}	3.3/2.8	VDW
Asp-223 OD1	$O3'_A$	2.5/2.6	H-bond
Asp-223 OD2	$O2'_A$	2.6/2.5	H-bond
Lys-228 NZ	$O3'_A$	3.1/2.9	H-bond
Ile-269 O	$O3'_N$	2.9/2.7	H-bond
Val-292 O	$N2_N$	3.2/3.2	VDW
Val-292 O	$N7_N$	3.1/3.3	H-bond
Ala-317 O	$N7_N$	3.0/3.2	H-bond
Ile-318 CA	$O7_N$	3.1/3.3	VDW
Phe-319 N	$O7_N$	2.9/2.8	H-bond
Arg-369 NH1	O_{P1N}	3.6/3.1	H-bond

[a] Contacts are listed in the order subunit A/subunit B. [b] This solvent molecule is not observed in subunit A.

(below). However, the zinc coordination geometry in the CNAD complex remains that of a distorted tetrahedron. Ligand lengths and angles subtended at the active site zinc atom are similar to those observed previously, with the exception of the His-67–Zn–pyridine angle (Table 5). This bond angle (136°) is significantly larger than those subtended between zinc and solvent or substrate in other complexes (88–101°). This is due to the restrictions on the movement of the CNAD pyridine ring discussed above.

(*d*) *CPAD Closely Mimics NADH Binding to LADH.* In contrast to the binding of CNAD, CPAD binds to LADH in a conformation very similar to that observed for NADH in the LADH–NADH–DMSO complex (Eklund et al., 1981, 1984). One CPAD molecule binds at the cofactor site on each LADH monomer. The CPAD-omitted $F_o - F_c$ map from subunit A of dimeric LADH is shown in Figure 2b. The corresponding map from subunit B is of equal quality.

When the Cα atoms of LADH in both the NADH–DMSO and CPAD–ethanol complexes are overlapped, the RMS difference betweenn CPAD and NADH is 0.4 Å. The similarities between the conformation of LADH-bound CPAD and that of LADH-bound NADH (Eklund et al., 1984) are clearly seen in Figure 3b and Table 3. Most differences in torsion angles between the two LADH-bound dinucleotides are within experimental error (Table 3).

Kinetic measurements show that CPAD lacks CNAD's high affinity and specificity for LADH, binding with an affinity comparable to that of regular cofactor (Goldstein et al., 1994). Displacement of the pyridine nitrogen in CPAD away from the Zn cation precludes the formation of an intermolecular coordination ligand, accounting for the weaker binding of CPAD relative to CNAD. This is illustrated in the CPAD-omitted $2F_o - F_c$ map (Figure 4b). Note, however, that CPAD does conserve the three carboxamide hydrogen bonds to the enzyme (Figure 4b, Table 4b), maintaining the complex in the closed form.

(*e*) *Alcohol Coordinates to the Active Site Zinc in the CPAD Complex.* As noted, the conformation of LADH-bound CPAD closely mimics that of NAD. Thus, the fourth coordination site on the catalytic zinc is free for occupation by water or substrate. Data suggest that this site is occupied by substrate.

As discussed in Experimental Procedures, a large peak on initial $F_o - F_c$ maps was observed near the catalytic zinc, which could not be completely accounted for by a single water molecule (Figure 6a). The presence of 14% ethanol in the crystallization medium suggested that this peak resulted from bound ethanol.

In order to confirm that an alcohol can bind to the active site zinc in the presence of CPAD, crystals of the complex grown in ethanol were soaked in (*S*)-(+)-2-pentanol. In general, the alcohol that places a longer aliphatic chain in the hydrophobic substrate channel binds more tightly (Sekhar & Plapp, 1990; Adolph et al., 1991). Data were obtained at 2.9 Å on the isomorphous crystals (see Experimental Procedures). Data from the pentanol-soaked crystals showed a significant increase in difference density at the substrate binding site relative to that seen in the original ethanol-containing complex (Figure 6b). This suggests that alcohol does bind at the substrate site in the presence of CPAD.

The general binding mode of ethanol in the LADH–CPAD complex is similar to that observed in other ternary complexes between LADH, cofactor or cofactor analogues, and substrate or substrate analogues (Eklund et al., 1982a,b, 1984; Cedergren-Zeppezauer et al., 1982; Ramaswamy et al., 1994). One ethanol molecule is bound to the active site zinc atom in each subunit in the CPAD complex. The alcohol sits in the substrate channel. The hydroxyl oxygen coordinates with the catalytic Zn, completing the roughly tetrahedral geometry about the cation (Figure 7a, Table 5).

In its coordinating position, the ethanol hydroxyl oxygen forms a bridging hydrogen bond to OG of Ser-48 (Figure 6a and 7a). As a result, OG of Ser-48 is shifted 1.6 Å "up" toward the Zn cation, relative to its position in the NADH–DMSO complex (Eklund et al., 1984) and in the CNAD–ethanol complex (below). A similar Ser-48 side-chain geometry is observed in other ternary LADH complexes containing bound alcohol (Eklund et al., 1982a; Ramaswamy et al., 1994). In these cases, the substrate or substrate analogue serves as a link between the active site Zn and Ser-48. This bond forms part of the proposed relay system which transfers

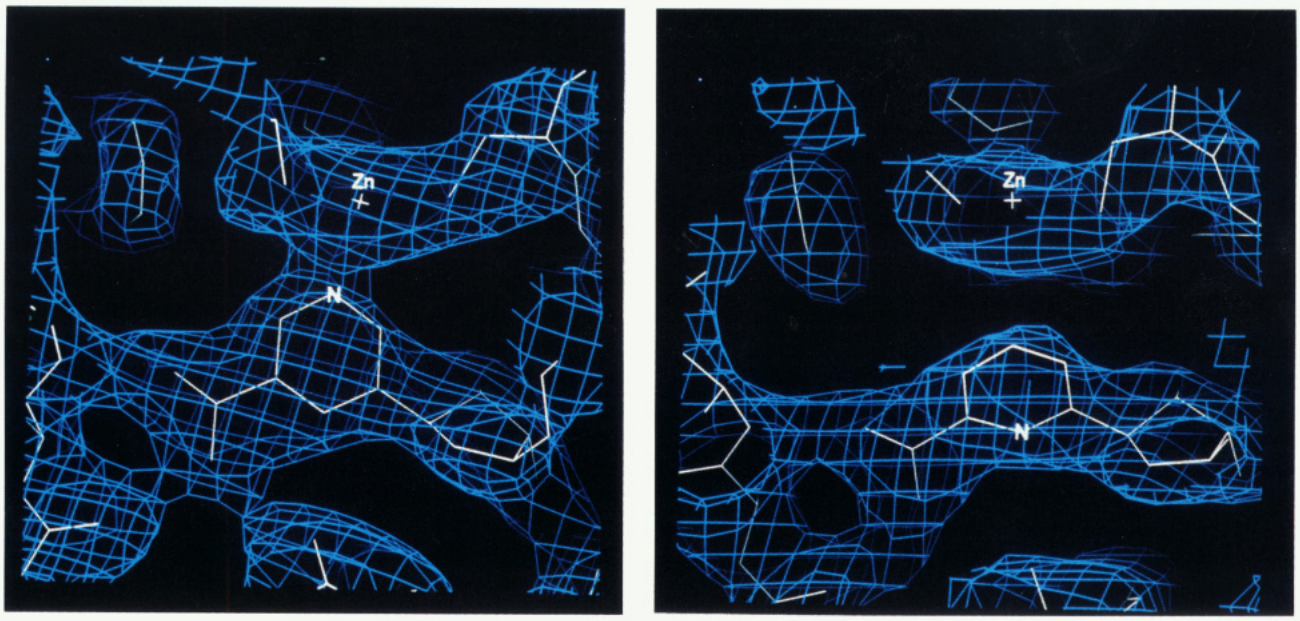

FIGURE 4: $2F_o - F_c$ map in the region of the LADH catalytic site in the (a, left) CNAD and (b, right) CPAD complexes. Maps are calculated from the final models with the inhibitors omitted and are contoured in blue at the 1.0 σ level. The LADH catalytic zinc and the inhibitor pyridine nitrogen are labeled. Models are shown in white. Note the continuous density between Zn and N in the CNAD complex (left). Bound substrate lies behind the zinc cation in each view and is not shown (see Figure 6).

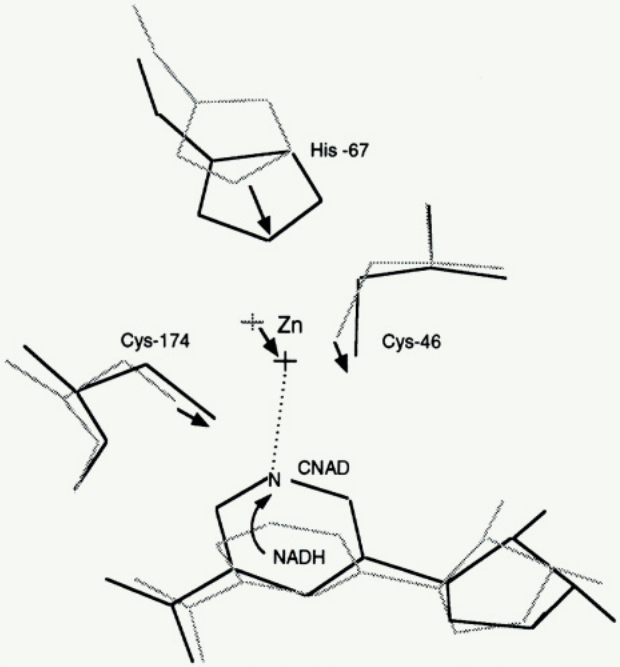

FIGURE 5: Geometry of the LADH catalytic site in the CNAD complex (dark bonds) compared with that in the NADH complex (light bonds; Eklund et al., 1984). Zinc cations are represented as crosses. Arrows indicate the rotation of the CNAD pyridine ring relative to that of the nicotinamide moiety, as well as the shift in the CNAD zinc coordination sphere. The resulting zinc–nitrogen ligand is 2.2 Å (dashed line). The overlap was obtained by superposition of the Cα atoms of the two complexes.

a proton from the buried alcohol substrate to solvent (Kvassman & Pettersson, 1978; Cook & Cleland, 1981; Eklund et al., 1982a; Sekhar & Plapp, 1990; Ehrig et al., 1991). Hydrogen bonds observed between Ser-48, the pyridine ribose 2′-hydroxyl oxygen, and solvent-accessible His-51 complete the proton abstraction system.

At the current resolution, the orientation of the ethanol molecule cannot be further defined. Two general models, based on the binding of slow reacting alcohols and substrate analogues, are proposed (Eklund et al., 1982a; Ramaswamy et al., 1994). In both models, the hydroxyl group remains coordinated with the zinc atom and hydrogen bonded to Ser-48. In one model, the ethanol binds with its *pro-R* hydrogen pointing away from the $C4_N$ atom of the CPAD pyridine ring. This model would require a rotation of the ethanol around the O1–C2 virtual axis in order for hydride transfer to occur. The second model places the ethanol *pro-R* hydrogen near the $C4_N$ atom of the pyridine ring of CPAD for direct hydride transfer (Figure 7a).

Higher resolution data will provide details of ethanol and pentanol binding to the LADH–CPAD complex. However, the similarity between CPAD and cofactor binding suggests that LADH–CPAD–alcohol structures will provide good models for the study of active ternary complex geometries.

(*f*) *CNAD Replaces Ethanol at the Active Site Zinc.* In the LADH–CNAD–ethanol complex, density corresponding to an ethanol molecule is located in the substrate binding channel, 4 Å away from the zinc atom (Figure 6c). As noted above, in the CPAD and other closed-form LADH complexes, the substrate or substrate analogue binds ~2 Å from the active site Zn, forming the fourth coordination ligand (Eklund et al., 1982a,b, 1984; Cedergren-Zeppezauer et al., 1982; Ramaswamy et al., 1994). In the LADH–CNAD complex, the CNAD pyridine nitrogen replaces ethanol in the zinc coordination sphere.

The methyl group of the ethanol can be modeled into a hydrophobic site surrounded by Phe-93, Leu-116, Val-294, and the pyridine ring of the CNAD (Figure 7b). Despite the increased distance between the ethanol molecule and the active site zinc, the ethanol hydroxyl group is still positioned to form a hydrogen bond with OG of Ser-48 in the active site (Figure 6c). In other alcohol-containing structures, this bond forms part of the proposed substrate–proton abstraction system (see above) (Eklund et al., 1982a). However, in the CNAD complex, the side chain of Ser-48 occupies an orientation different from that observed in the CPAD complex and other alcohol-containing structures (Figure 6c). In the CNAD complex, displacement of the bound substrate results in the Ser-48 pointing "down", i.e., away from the catalytic zinc. A

Table 5: Comparison of Coordination Geometry of the Active Site Zinc Atom in the CNAD, CPAD, and NADH Complexes

residue and atom name	distance from Zn (Å)[a]			
	LADH–CNAD	LADH–CPAD	LADH–NADH (ternary)	LADH (binary)
Cys-46 SG (S46)	2.3	2.2	2.4	2.4
His-67 NE2 (N67)	2.0	2.0	2.3	2.2
Cys-174 SG (S174)	2.3	2.0	2.3	2.4
fourth ligand[b]	2.2	2.1	2.1	2.2
residue and atom name	**angles subtended at Zn (deg)**			
	LADH–CNAD	LADH–CPAD	LADH–NADH (ternary)	LADH (binary)
S46–Zn–N67	106	110	107	113
S46–Zn–S174	125	130	138	127
N67–Zn–S174	97	102	109	105
S46–Zn–ligand	97	99	110	108
N67–Zn–ligand	136	89	88	101
S174–Zn–ligand	98	117	94	100

[a] Data for the ternary structure is from the LADH–NADH–DMSO complex (Eklund et al., 1984). Data for the binary complex is from the apo-LADH structure (Eklund et al., 1976). [b] The fourth ligand refers to the electron-donating atom on the substrate, substrate analogue, or inhibitor. In the LADH–CNAD complex, the fourth ligand is $N5_N$ of the CNAD pyridine ring.

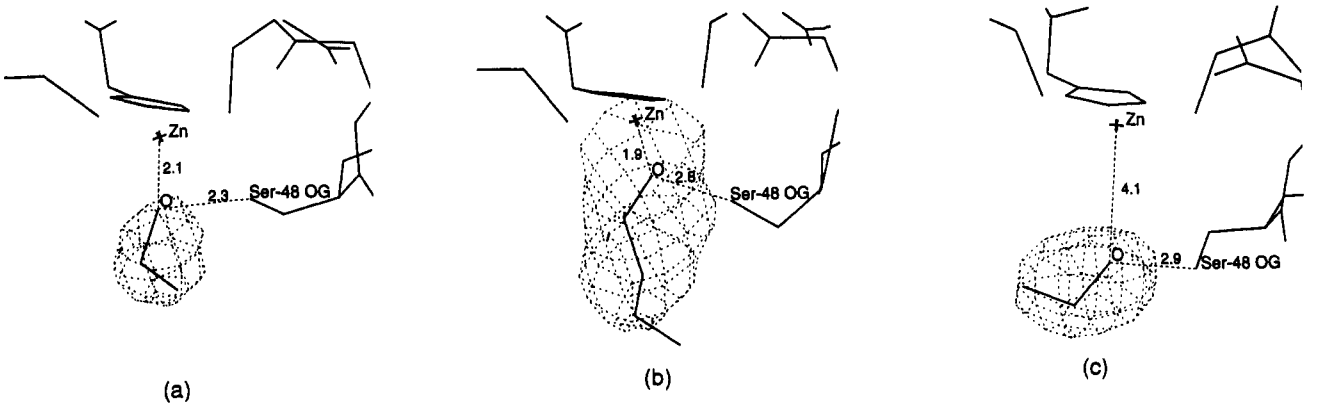

FIGURE 6: $F_o - F_c$ maps at the substrate binding site in the (a) CPAD–ethanol, (b) CPAD–pentanol, and (c) CNAD–ethanol complexes. All maps are contoured at the 3σ level. The map for the CNAD complex is from subunit A, and those for the CPAD complexes are from subunit B. However, distances shown in angstroms for each complex are averages of the refined models from both subunits. The catalytic zinc is indicated by the cross.

similar Ser-48 geometry is observed in the LADH–NADH–DMSO complex (Eklund et al., 1984).

SUMMARY AND DISCUSSION

The binding of two neutral and isosteric analogues of NAD to LADH is presented. Final models for the catalytic site geometries in both complexes are illustrated in Figure 7.

Both CNAD and CPAD mimic normal cofactor binding to LADH to an extent sufficient to induce the conformational transition from the open to the closed form of the enzyme. All hydrogen-bonding interactions observed previously between cofactor and enzyme are conserved in both inhibitor complexes, including hydrogen bonds to the pyridine carboxamide groups.

The inhibitor CPAD binds to LADH in a conformation almost identical to that of the normal cofactor. This is consistent with kinetic studies, which show similar K_i's for NADH and CPAD (Goldstein et al., 1994). The pyridine nitrogen in CPAD is remote from the active site zinc. Examination of ethanol and pentanol ternary complexes suggests that alcohol provides the fourth coordination ligand to the active site zinc (Figure 7a).

Only one other NAD analogue has yielded a closed-form complex with LADH. This is 1,4,5,6-tetrahydronicotinamide adenine dinucleotide (Cedergren-Zappezauer et al., 1982), an inhibitor with a slightly puckered heterocycle (Cedergren-Zappezauer, 1986). Other structural studies of substrate binding to ternary complexes of LADH have employed normal cofactor with substrate inhibitors or slowly reacting alcohols (Plapp et al., 1978; Eklund et al., 1982a; Ramaswamy et al., 1994).

Alcohols bound to the LADH–CPAD complex are not oxidized. Thus, ternary complexes using CPAD as a coenzyme analogue do not have limitations on the type of substrates used. Given the similarity of CPAD and cofactor binding to LADH, LADH–CPAD–alcohol complexes provide a potentially useful model system for the study of alcohol binding. Further, both CPAD and CNAD are general dehydrogenase inhibitors (Goldstein et al., 1994), suggesting that these analogues may find use in the study of ternary complexes involving other NAD–dependent enzymes.

Unlike CPAD, the inhibitor CNAD shows high affinity and specificity for LADH (Goldstein et al., 1994). The difference in binding free energy between CNAD and CPAD in LADH is approximately 5 kcal/mol, based on measured binding and dissociation constants (Goldstein et al., 1994). The structure of the ternary CNAD complex indicates that the electron-donating pyridine nitrogen of CNAD provides the fourth coordination ligand to the active site zinc (Figure 7b). In contrast, the pyridine nitrogen in LADH-bound CPAD does not participate in any specific interactions (Figure 7a). The enthalpy of the Zn···N ligand is by itself sufficient to account for much of the difference in affinity between CNAD and CPAD, assuming that the two inhibitors have similar solvation energies (Goldstein et al., 1994; Martell & Smith,

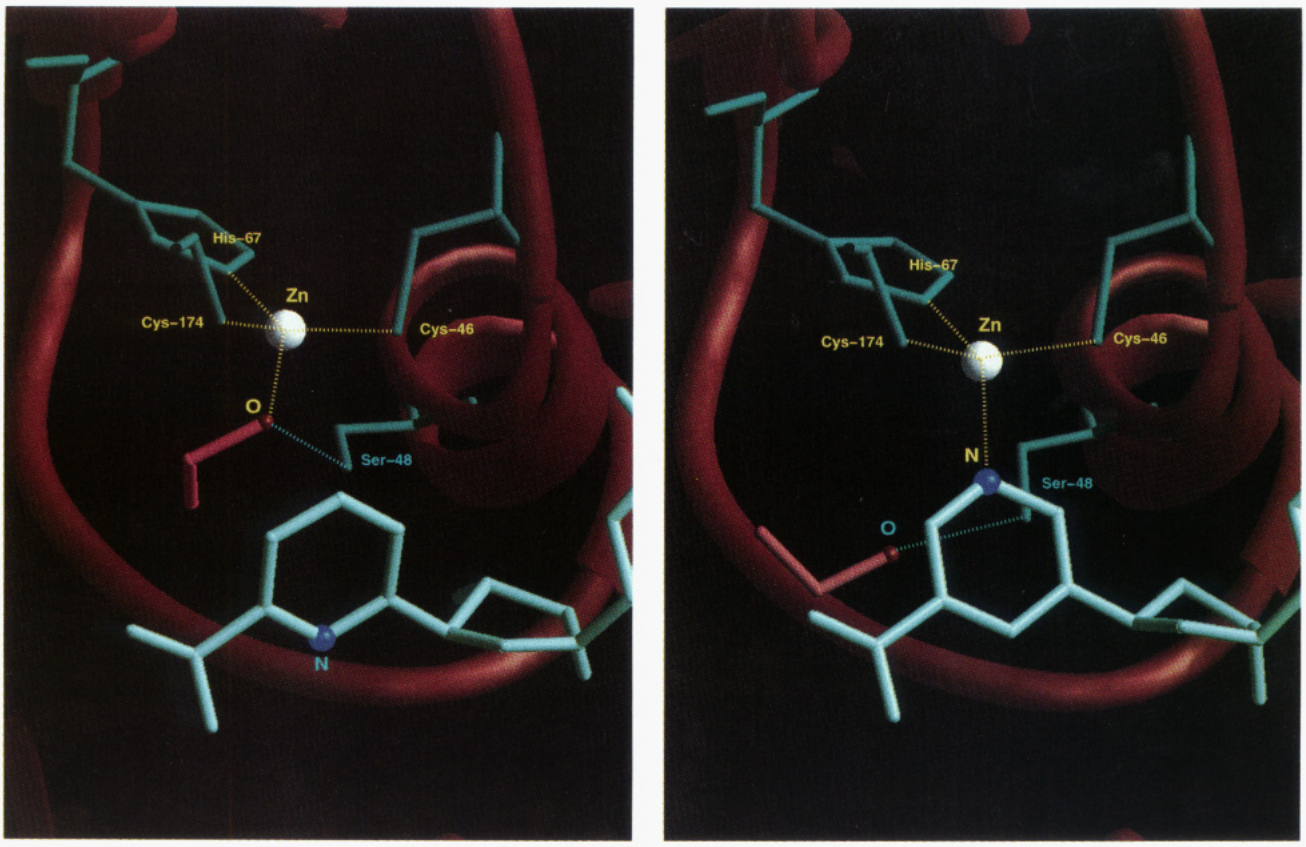

FIGURE 7: Comparison of final models in the region of the LADH catalytic site in the (a, left) CPAD and (b, right) CNAD complexes. Hydrogen bonds and coordination ligands are represented as yellow dashed lines. Each model shows the pyridine end of the inhibitor (light blue) and active site residues (blue) binding the catalytic zinc (white sphere) and alcohol (red). Note the difference in the fourth coordination ligand to the zinc and the position of the alcohol between the two complexes.

1989). However, differences in both the enthalpic and entropic costs of ligation and isomerization between the two complexes can be significant (Jencks, 1975). In the CNAD complex, the Zn···N coordination is facilitated by rotation of the CNAD pyridine ring toward the zinc atom, as well as a shift of the zinc coordination sphere toward the pyridine ring. Occupation of the fourth zinc ligand by CNAD blocks alcohol coordination to the active site zinc (Figure 7b). These results are consistent with kinetic and computational studies, which suggest that CNAD interferes with both NAD binding in the cofactor pocket and ethanol binding to the active site zinc (Goldstein et al., 1994).

Like CNAD, other potent reversible inhibitors of LADH bind to the catalytic zinc atoms. These include 4-substituted alkylpyrazoles (Dahlbom et al., 1974; Fries et al., 1979; Tolf et al., 1979), 1-mercapto-*n*-alkanes (Miwa et al., 1987), phenylacetamide and formamide derivatives (Freudenreich et al., 1984), and aldoximes (Sigman et al., 1982). However, these compounds act as substrate analogues, binding Zn from the substrate site, with alkyl or phenyl groups extending into the hydrophobic substrate cleft (Eklund et al., 1982b; Miwa et al., 1987; Sigman et al., 1982; Freudenreich et al., 1984). CNAD represents a new class of "hybrid" alcohol dehydrogenase inhibitor, a hydride-resistant cofactor analogue that directly ligates to the catalytic zinc.

ACKNOWLEDGMENT

The authors are indebted to Dr. H. L. Carrell for his considerable aid in the data collection and to Dr. Jenny P. Glusker for the use of her diffraction facility. The authors thank Drs. Jeffrey P. Jones, Bryce V. Plapp, and Carol Stone for useful discussions.

SUPPLEMENTARY MATERIAL AVAILABLE

A list of cross-rotational search peaks, a contour plot of the self-rotation function for the LADH–CNAD complex, Luzzati and Ramachandran plots from the LADH–CNAD and LADH–CPAD structures, and stereoviews of Figures 3 and 5 (8 pages). Ordering information is given on any current masthead page.

REFERENCES

Abdallah, M. A., Biellmann, J.-F., Nordström, B., & Brändén, C.-I. (1975) *Eur. J. Biochem. 50*, 475–481.
Adolph, H. W., Maurer, P., Schneider-Bernlöhr, H., Sartorius, C., & Zeppezauer, M. (1991) *Eur. J. Biochem. 201*, 615–625.
Baud, F. J., Bismuth, C., Garnier, R., Galliot, M., Astier, A., Maistre, G., & Soffer, M. (1987) *Clin. Toxicol. 24*, 463–483.
Bernstein, F. C., Koetzle, T. F., Williams, G. J. B., Meyer, E. F., Brice, M. D., Rodgers, J. R., Kennard, O., Shimanouchi, T., & Tasumi, M. (1977) *J. Mol. Biol. 112*, 535–542.
Biellmann, J.-F., Samama, J.-P., Brändén, C.-I., & Eklund, H. (1979) *Eur. J. Biochem. 102*, 107–110.
Brünger, A. T. (1990) *Acta Crystallogr. A46*, 46–57.
Brünger, A. T. (1992a) *X-PLOR version 3.0 Manual*, Yale University, New Haven, CT.
Brünger, A. T. (1992b) *Nature 355*, 472–475.
Brünger, A. T., Krukowski, A., & Erickson, J. W. (1990) *Acta Crystallogr. A46*, 585–593.
Cedergren-Zeppezauer, E. (1983) *Biochemistry 22*, 5761–5772.
Cedergren-Zeppezauer, E. S. (1986) in *Zinc Enzymes* (Bertini, I., Luchinat, C., Maret, W., & Zeppezauer, M., Eds.) Chapter 29, Birkhäuser, Boston, MA.

Cedergren-Zeppezauer, E., Samama, J. P., & Eklund, H. (1982) *Biochemistry 21*, 4895–4908.
Cook, P. F., & Cleland, W. W. (1981) *Biochemistry 20*, 1805–1816.
Crow, K. E., & Hardman, M. J. (1989) in *Human Metabolism of Alcohol. Vol. 2: Regulation, Enzymology and Metabolites of Ethanol* (Crow, K. E., & Batt, R. D., Eds.) Chapter 1, CRC Press, Boca Raton, FL.
Dahlbom, R., Tolf, B.-R., Akeson, A., Lundquist, G., & Theorell, H. (1974) *Biochem. Biophys. Res. Commun. 57*, 549–553.
Dalziel, K., & Dickinson, F. M. (1975) *Enzymes (3rd Ed.) 11*, 1–60.
Danenberg, P. V., Danenberg, K. D., & Cleland, W. W. (1978) *J. Biol. Chem. 253*, 5886–5887.
Ehrig, T., Hurley, T. D., Edenberg, H. J., & Bosron, W. F. (1991) *Biochemistry 30*, 1062–1068.
Einarsson, R., Eklund, H., Zeppezauer, E., Boiwe, T., & Brändén, C.-I. (1974) *Eur. J. Biochem. 49*, 41–47.
Eklund, H., & Brändén, C.-I. (1987a) in *Biological Macromolecules and Assemblies. Vol. 3: Active Sites of Enzymes* (Jurnak, F. A., & McPherson, A., Eds.) Chapter 2, John Wiley and Sons, New York.
Eklund, H., & Brändén, C.-I. (1987b) in *Pyridine Nucleotide Coenzymes. Chemical, Biochemical, and Medical Aspects* (Dolphin, D., Avramovic, O., & Poulson, R., Eds.) Vol. II, Part A, Chapter 4, John Wiley and Sons, New York.
Eklund, H., Nordström, B., Zeppezauer, E., Söderlund, G., Ohlsson, I., Boiwe, T., Soderberg, B. O., Tapia, O., & Brändén, C.-I. (1976) *J. Mol. Biol. 102*, 27–59.
Eklund, H., Samama, J.-P., Wallén, L., Brändén, C.-I., Akeson, A., & Jones, T. A. (1981) *J. Mol. Biol. 146*, 561–587.
Eklund, H., Plapp, B. V., Samama, J.-P., & Brändén, C.-I. (1982a) *J. Biol. Chem. 257*, 14349–14358.
Eklund, H., Samama, J.-P., & Wallén, L. (1982b) *Biochemistry 21*, 4858–4866.
Eklund, H., Samama, J.-P., & Jones, T. A. (1984) *Biochemistry 23*, 5982–5996.
Freudenreich, C., Samama, J.-P., & Biellmann, J.-F. (1984) *J. Am. Chem. Soc. 106*, 3344–3353.
Fries, R. W., Bohlken, D. P., & Plapp, B. V. (1979) *J. Med. Chem. 22*, 356–359.
Goldstein, B. M., Bell, J. E., & Marquez, V. E. (1990) *J. Med. Chem. 33*, 1123–1127.
Goldstein, B. M., Li, H., Jones, J. P., Bell, J. E., Zeidler, J., Pankiewicz, K., & Watanabe, K. A. (1994) *J. Med. Chem. 37*, 392–399.
Hodel, A., Kim, S.-H., & Brünger, A. T. (1992) *Acta Crystallogr. A48*, 851–858.
Huber, R. (1985) in *Molecular Replacement, Proceedings of the Daresbury Study Weekend*, February 1985, pp 58–61, SERC Daresbury Laboratory, Warrington, England.
Hurley, T. D., Bosron, W. F., Hamilton, J. A., & Amzel, L. M. (1991) *Proc. Natl. Acad. Sci. U.S.A. 88*, 8149–8153.
Jacobsen, D., Sebastian, C. S., Barron, S. K., Carriere, E. W., & McMartin, K. E. (1990) *J. Emerg. Med. 8*, 455–461.
Jencks, W. P. (1975) in *Advances in Enzymology and Related Areas of Molecular Biology* (Meister, A., Ed.) Vol. 43, pp 219–410, John Wiley and Sons, New York.
Kabsch, W. (1988a) *J. Appl. Crystallogr. 21*, 67–71.
Kabsch, W. (1988b) *J. Appl. Crystallogr. 21*, 916–924.
Klinman, J. P. (1981) *CRC Crit. Rev. Biochem. 10*, 39–78.
Kvassman, J., & Pettersson, G. (1978) *Eur. J. Biochem. 87*, 417–427.
Kvassman, J., Larsson, A., & Pettersson, G. (1981) *Eur. J. Biochem. 114*, 555–563.
Li, H., Hallows, W. A., Punzi, J. S., Marquez, V. E., Carrell, H. L., Pankiewicz, K. W., Watanabe, K. A., & Goldstein, B. M. (1994) *Biochemistry 33*, 23–32.
Luzzati, P. V. (1952) *Acta Crystallogr. 5*, 802–81.
Martell, A. E., & Smith, R. M. (1989) *Critical Stability Constants*, Vol. 6, p 258, Plenum Press, New York.
Miwa, K., Okuda, H., Ogura, K., & Watabe, T. (1987) *Biochem. Biophys. Res. Commun. 142*, 993–998.
Pankiewicz, K. W., Zeidler, J., Ciszewski, L. A., Bell, J. E., Goldstein, B. M., Jayaram, H. N., & Watanabe, K. A. (1993) *J. Med. Chem. 36*, 1855–1859.
Plapp, B. V., Eklund, H., & Brändén, C.-I. (1978) *J. Mol. Biol. 122*, 23–32.
Ramachandran, G. N., & Sasisekharan, V. (1968) *Adv. Protein Chem. 23*, 283–437.
Ramaswamy, S., Eklund, H., & Plapp, B. V. (1994) *Biochemistry 33*, 5230–5237.
Rossmann, M. G., & Blow, D. M. (1962) *Acta Crystallogr. 15*, 24–31.
Sack, J. S. (1988) *J. Mol. Graphics 6*, 224–225.
Salaspuro, M. P., Pikkarainen, P., & Lindros, K. (1977) *Eur. J. Clin. Invest. 7*, 487–490.
Samama, J.-P., Zeppezauer, E., Biellmann, J.-F., & Brändén, C.-I. (1977) *Eur. J. Biochem. 81*, 403–409.
Samama, J.-P., Wrixon, A.-D., & Biellmann, J.-F. (1981) *Eur. J. Biochem. 118*, 479–486.
Sekhar, V. C., & Plapp, B. V. (1990) *Biochemistry 29*, 4289–4295.
Sigman, D. S., Frolich, M., & Anderson, R. E. (1982) *Eur. J. Biochem. 126*, 523–529.
Tolf, B.-R., Piechaczek, J., Dahlbom, R., Theorell, A., Akeson, A., & Lundquist, G. (1979) *Acta Chem. Scand. B33*, 483–487.
Weis, W. T., Brunger, A. T., Skehel, J. J., & Wiley, D. C. (1990) *J. Mol. Biol. 212*, 737–761.
Woenckhaus, C., & Jeck, R. (1987) in *Pyridine Nucleotide Coenzymes. Chemical, Biochemical, and Medical Aspects* (Dolphin, D., Avramovic, O., & Poulson, R., Eds.) Vol. II, Part A, Chapter 13, John Wiley and Sons, New York.
Zeppezauer, E., Söderberg, B.-O., Brändén, C.-I., Akeson, A., & Theorell, H. (1967) *Acta Chem. Scand. 21*, 1099–1101.